Journal of the Association of Arab Universities for Basic and Applied Sciences (2017) **23**, 66–74

University of Bahrain

Journal of the Association of Arab Universities for Basic and Applied Sciences

www.elsevier.com/locate/jaaubas
www.sciencedirect.com

ORIGINAL ARTICLE

Fully developed flow of non-Newtonian fluids in a straight uniform square duct through porous medium

M. Devakar *, K. Ramesh, Sagar Chouhan, Ankush Raje

Department of Mathematics, Visvesvaraya National Institute of Technology, Nagpur 440010, India

Received 13 August 2014; revised 7 February 2016; accepted 3 April 2016
Available online 11 May 2016

KEYWORDS

Couple stress fluid;
Jeffrey fluid;
Square duct;
Porous medium;
Finite difference method

Abstract In this paper, we have studied the flow of incompressible fluids in a straight square duct through the porous medium. The couple stress fluid model and Jeffrey fluid model are considered separately to study the flow properties. The governing partial differential equations have been solved numerically using finite difference method in each case. In both the cases, the variation of different flow parameters on the fluid velocity is illustrated graphically and the numerical results for the volume flow rate have been presented through tables. It is observed that, the velocity and volume flow rate decrease with an increase in couple stress parameter and porosity parameter, while the velocity and volume flow rate increase with an increase in Jeffrey parameter and pressure gradient.

1. Introduction

The study of non-Newtonian fluids is very important because of its applications in several industrial and engineering processes. Many materials such as drilling mud, blood, ketchup, tooth-paste, certain oils and greases, polymer melts and many other emulsions have been treated as non-Newtonian fluids. Due to vast variety in the physical structure of real fluids, it is not easy to propose a single constitutive equation which exhibits all properties of real fluids. Therefore, a number of non-Newtonian fluid models have been proposed to predict the behavior of real fluids. Due to its diverse applications, many authors have studied the non-Newtonian fluid flows in different geometries (see Radhakrishnamacharya, 1977; Rao, 1999; Vajravelu et al., 2002; Fetecau and Fetecau, 2005; Kothandapani and Srinivas, 2008; Firouzi and Hashemabadi, 2009; Khan et al., 2010; Liu et al., 2011; Mukhopadhyay and Bhattacharyya, 2012; Ellahi, 2013; Devakar, 2013; Hayat et al., 2013a,b). A comprehensive review of fluids of differential type and their applications is made by Ellahi (2014).

The couple stress fluid model initiated by Stokes (1984) presents a simple generalization of the classical viscous Newtonian model which allows for polar effects such as the presence of couple stresses and body couples in the fluid medium. The important feature of this fluid is that, the stress tensor is not symmetric. The equations governing the couple stress fluid flow are of higher order than the classical Navier–Stokes equations and offer challenges to the researchers working in this field. The study of couple stress fluid is very useful in understanding

* Corresponding author.
E-mail address: m_devakar@yahoo.co.in (M. Devakar).
Peer review under responsibility of University of Bahrain.

http://dx.doi.org/10.1016/j.jaubas.2016.04.001

various physical problems because it possesses the mechanism to describe the rheological complex fluids such as liquid crystals, lubricants containing small amount of polymer additive and human blood. In view of this, several researchers have made their contributions to the study of couple stress fluid flow problems. Devakar and Iyengar (2008) have discussed Stokes' first and second problems for an incompressible couple stress fluid. Srinivasacharya et al. (2009) have discussed the flow and heat transfer of couple stress fluid in a porous channel with an expanding and contracting wall. Ramana Murthy et al. (2010) have presented finite difference solution for MHD flow of couple stress fluid between two concentric rotating cylinders with porous lining. Devakar and Iyengar (2010) have studied the run up flow of an incompressible couple stress fluid between parallel plates. Farooq et al. (2013) have studied the non-isothermal Poiseuille flow between two heated parallel inclined plates using incompressible couple stress fluid. Devakar et al. (2014) have obtained analytical solutions of couple stress fluid flows between parallel plates with slip boundary conditions. Recently, Ramesh and Devakar (2015) have discussed the effects of magnetic field and heat transfer on the peristaltic flow of an incompressible couple stress fluid through porous medium in an inclined asymmetric channel.

Another non-Newtonian fluid model that has attracted the attention of researchers in fluid dynamics is the Jeffrey fluid model which describes the effects of the ratio of relaxation to retardation times and retardation time. Kothandapani and Srinivas (2008) have studied the peristaltic transport of a Jeffrey fluid under the effect of magnetic field in an asymmetric channel. Qayyum et al. (2012) have discussed the unsteady squeezing flow of Jeffery fluid between two parallel disks. Akbar and Nadeem (2012) have analyzed the simulation of variable viscosity and Jeffrey fluid model for blood flow through a tapered artery with a stenosis. Ellahi et al. (2013) have discussed three-dimensional stretched flow of Jeffrey fluid with variable thermal conductivity and thermal radiation.

The flow through porous medium is of fundamental importance in geomechanics, biomechanics and industry. The applications in which flow through a porous medium is mostly prominent are filtration of fluids, seepage of water in river beds, movement of underground water and oils, functioning of human lung, physiological fluid flow in bile duct and gall-bladder with stones, and flow of blood through small blood vessels. Aforementioned applications inspired the researchers to investigate the flows through porous medium in different geometries. Afifi and Gad (2001) have made a theoretical study on the interaction of peristaltic flow with pulsatile magneto-fluid through a porous medium. Murthy et al. (2004) have discussed the effect of double stratification on free convection in Darcian porous medium. Zeeshan and Ellahi (2013) have studied the effect of heat transfer and magnetic field on the third grade fluid in a pipe with porous space. A few more studies on the flows through porous medium for diverse situations are made by Prasad and Kumar (2011), Tripathi (2002), Ellahi et al. (2013) and Sheikholeslami et al. (2014).

The flow of fluid in a square duct is one of the most important flows in fluid mechanics because of its applications in industry and medicine. The applications include supply of fluids via pipe lines in the oil and petrochemical industries, food production, the fabrication of chemical materials, medical applications, and the injection of polymeric materials. The flow through a straight duct of square cross section was reported by Williams and Baker in 1966 (Johnson, 1998). Rahman and Ahmad (1982) have presented finite element analysis of axial flow with heat transfer in a square duct. Cook and Rahman (1986) have presented exact solutions of the temperature and velocity distributions for the Newtonian fluid flow through a square duct. Subsequently, many authors have studied the flow problems through the ducts of square cross section. Sayed-Ahmed (2000) discussed the laminar heat transfer for thermally developing flow of a Herschel–Bulkley fluid in a square duct. Beale (2005) studied the effect of mass transfer on Newtonian fluid in square duct. Adachi (2006) discussed the stability of natural convection in an inclined square duct with perfectly conducting side walls. Zhang et al. (2007) have presented the numerical study of flow of Oldroyd-3-Constant fluid in a straight duct with square cross-section. Lee (2008) studied the convective heat transfer to water near the critical region in a horizontal square duct. Norouzi et al. (2010) have investigated the inertial and creeping flow of a second-order fluid in a curved duct with a square cross-section. Heris et al. (2011) have made an experimental study on the forced convective heat transfer through square cross-sectional duct under laminar flow regime using CuO/water nanofluid. Tympel et al. (2012) have investigated the distortion of liquid metal flow in a square duct due to the influence of a magnetic point dipole. Sarma et al. (2014) have presented a numerical study for steady MHD flow of liquid metal through a square duct under the action of strong transverse magnetic field. Kun et al. (2014) have investigated experimentally the study of pseudoplastic fluid flows in a square duct of strong curvature. Ting and Hou (2015) have numerically investigated the convective heat transfer of water-based Al_2O_3 nanofluid flowing through a square cross-section duct with a constant heat flux under laminar flow conditions.

The fully developed flow through straight uniform square duct has not been studied so far neither for couple stress fluid nor for Jeffrey fluid. The aim of present paper is to investigate the flow of couple stress fluid and Jeffrey fluid in a straight duct of uniform square cross section separately. The channel is filled with homogeneous porous medium. The Cartesian coordinate system has been considered. We find the numerical solution of the governing partial differential equations using finite difference method. The graphical results are presented for velocity profile with various involved fluid parameters for both problems.

2. Formulation of the problem

Consider the steady flow of an incompressible non-Newtonian fluid through a straight square porous duct with uniform square cross-section. We choose the Cartesian coordinate system such that the z-axis along the axis of the duct and x, y-axes along the sides of square duct. Let $x = a$ and $y = a$ be the lengths of the square duct in x and y directions respectively. The fluid is set into motion by a constant pressure gradient in the positive z-direction so that the flow occurs only in z-direction (see Fig. 1). Since the flow is along the z-direction, the velocity at any point in the flow field is expected to be in the form $\bar{q} = (0, 0, w(x, y))$. The equations governing the flow of an incompressible non-Newtonian fluid through the porous medium are given by Nadeem and Akram (2010) and Tripathi (2002)

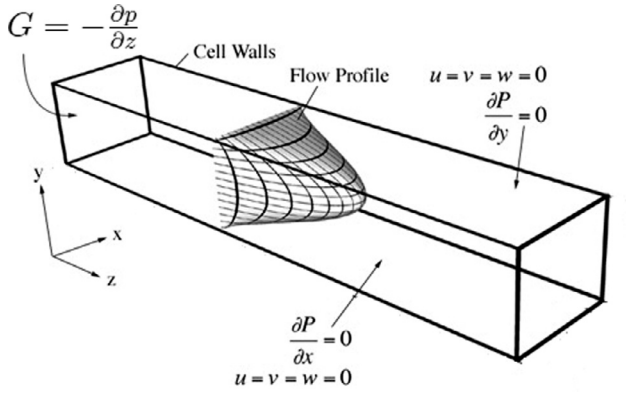

Fig. 1 Geometry of the problem.

$$\nabla \cdot \bar{q} = 0, \tag{1}$$

$$\rho\left(\frac{\partial \bar{q}}{\partial t} + \bar{q} \cdot \nabla \bar{q}\right) = \rho \bar{F} + \nabla \cdot \tau + R, \tag{2}$$

where $\bar{q}$ is the velocity vector, ρ is the density, $\bar{F}$ is the body force per unit mass, τ is the stress tensor and R is the Darcy resistance and it is given as

$$R = -\frac{\mu}{k}\bar{q}, \tag{3}$$

where k is the permeability parameter.

2.1. Couple stress fluid model

The constitutive equations concerning the force stress tensor τ and the couple stress tensor M^* that arise in the theory of couple stress fluids are given by

$$\tau = (-p + \lambda^* \nabla.\bar{q})I + \mu\left[\nabla \bar{q} + (\nabla \bar{q})^T\right] + \frac{1}{2} I \times [\nabla . M^* + \rho C], \tag{4}$$

$$M^* = mI + 2\eta \nabla(\nabla \times \bar{q}) + 2\eta'(\nabla(\nabla \times \bar{q}))^T. \tag{5}$$

In the above m is $\frac{1}{3}$ trace of M^*, μ and λ^* are the viscosity coefficients, C is the body couple vector and η, η' are the couple stress viscosity coefficients. These material constants are constrained by the inequalities

$$\mu \geqslant 0, \quad 3\lambda^* + 2\mu \geqslant 0, \quad \eta \geqslant 0, \quad |\eta'| \leqslant \eta. \tag{6}$$

The choice of velocity $\bar{q} = (0, 0, w(x, y))$ automatically satisfies the continuity equation (1) and the momentum equation (2) takes the form

$$\mu \nabla^2 w - \eta \nabla^4 w - \frac{\mu}{k} w - \frac{\partial p}{\partial z} = 0, \tag{7}$$

where $\nabla^2 = \frac{\partial^2}{\partial x^2} + \frac{\partial^2}{\partial y^2}$ and $\nabla^4 = \nabla^2 \nabla^2$.

The boundary conditions for this flow are

$$\left.\begin{aligned} w(x,0) = 0 = w(x,a) \quad \text{for } 0 \leqslant x \leqslant a \\ w(0,y) = 0 = w(a,y) \quad \text{for } 0 \leqslant y \leqslant a \end{aligned}\right\}, \tag{8}$$

(No-slip boundary conditions)

$$\frac{\partial w}{\partial x} = \frac{\partial w}{\partial y} \text{ on the boundary. (Hyperstick boundary condition)} \tag{9}$$

Introducing the non-dimensional variables

$$\bar{x} = \frac{x}{a}, \quad \bar{y} = \frac{y}{a}, \quad \bar{z} = \frac{z}{a}, \quad \bar{w} = \frac{\rho a}{\mu} w, \quad \bar{p} = \frac{\rho a^2}{\mu^2} p,$$
$$c^2 = \frac{\eta}{\mu a^2}, \quad \sigma^2 = \frac{a^2}{k}. \tag{10}$$

After simplification and dropping the bars, the Eq. (7) can be written as

$$\frac{\partial^4 w}{\partial x^4} + 2\frac{\partial^4 w}{\partial x^2 \partial y^2} + \frac{\partial^4 w}{\partial y^4} - \frac{1}{c^2}\left(\frac{\partial^2 w}{\partial x^2} + \frac{\partial^2 w}{\partial y^2}\right) + \frac{\sigma^2}{c^2} w = \frac{G}{c^2}, \tag{11}$$

in which $G = -\frac{\partial p}{\partial z}$, a constant.

The non-dimensional boundary conditions to be satisfied are

$$w(x,0) = 0 = w(x,1) \quad \text{for } 0 \leqslant x \leqslant 1, \tag{12}$$

$$w(0,y) = 0 = w(1,y) \quad \text{for } 0 \leqslant y \leqslant 1, \tag{13}$$

$$\frac{\partial w}{\partial x} = \frac{\partial w}{\partial y} \text{ on the boundary of the square duct.} \tag{14}$$

Though the non-homogeneous partial differential equation (11) is linear, it is not amenable for exact solution.

2.2. Jeffrey fluid model

The stress tensor for the Jeffrey fluid is given by

$$\tau = -pI + \frac{\mu}{1+\lambda_1}\left[\left((\nabla \bar{q}) + (\nabla \bar{q})^T\right) + \lambda_2 \frac{d}{dt}\left((\nabla \bar{q}) + (\nabla \bar{q})^T\right)\right], \tag{15}$$

where p is the pressure, I is the identity matrix, μ is the dynamic viscosity, λ_1 is the ratio of relaxation and retardation times, λ_2 is the retardation time.

The velocity $\bar{q} = (0, 0, w(x, y))$ satisfies the incompressibility condition and the momentum equation (2) can be written as

$$\frac{\mu}{1+\lambda_1}\left(\frac{\partial^2 w}{\partial x^2} + \frac{\partial^2 w}{\partial y^2}\right) - \frac{\partial p}{\partial z} - \frac{\mu}{k} w = 0. \tag{16}$$

The boundary conditions are given by

$$w(x,0) = 0 = w(x,a) \quad \text{for } 0 \leqslant x \leqslant a, \tag{17}$$

$$w(0,y) = 0 = w(a,y) \quad \text{for } 0 \leqslant y \leqslant a. \tag{18}$$

Introducing the non-dimensional variables

$$\bar{x} = \frac{x}{a}, \quad \bar{y} = \frac{y}{a}, \quad \bar{z} = \frac{z}{a}, \quad \bar{w} = \frac{\rho a}{\mu} w, \quad \bar{p} = \frac{\rho a^2}{\mu^2} p, \quad \sigma^2 = \frac{a^2}{k}. \tag{19}$$

After dropping the bars the Eqs. (16)–(18) become

$$\frac{\partial^2 w}{\partial x^2} + \frac{\partial^2 w}{\partial y^2} - \sigma^2(1+\lambda_1) w = -G(1+\lambda_1), \tag{20}$$

in which $G = -\frac{\partial p}{\partial z}$, a constant with the boundary conditions

$$w(x,0) = 0 = w(x,1) \quad \text{for } 0 \leqslant x \leqslant 1, \tag{21}$$

$$w(0,y) = 0 = w(1,y) \quad \text{for } 0 \leqslant y \leqslant 1. \tag{22}$$

3. Numerical solution of the problem

3.1. Couple stress fluid model

The momentum equation governing the flow (11) along with the boundary conditions (12)–(14) are solved numerically using finite difference method. The derivatives are replaced by the central difference approximations to obtain algebraic system and the classical Gauss elimination method is used to solve the resulting algebraic system of equations. The second order finite difference approximations of the higher order derivatives of w occurring in the momentum equation are given in the following:

$$\left(\frac{\partial^2 w}{\partial x^2}\right)_{i,j} = \frac{w_{i+1,j} - 2w_{i,j} + w_{i-1,j}}{h^2}, \tag{23}$$

$$\left(\frac{\partial^2 w}{\partial y^2}\right)_{i,j} = \frac{w_{i,j+1} - 2w_{i,j} + w_{i,j-1}}{k^2}, \tag{24}$$

$$\left(\frac{\partial^4 w}{\partial x^4}\right)_{i,j} = \frac{w_{i+2,j} - 4w_{i+1,j} + 6w_{i,j} - 4w_{i-1,j} + w_{i-2,j}}{h^4}, \tag{25}$$

$$\left(\frac{\partial^4 w}{\partial y^4}\right)_{i,j} = \frac{w_{i,j+2} - 4w_{i,j+1} + 6w_{i,j} - 4w_{i,j-1} + w_{i,j-2}}{k^4}, \tag{26}$$

where h, k are step sizes in x, y-directions respectively.

$$\left(\frac{\partial^4 w}{\partial x^2 \partial y^2}\right)_{i,j} = \frac{w_{i+1,j+1} - 2w_{i,j+1} + w_{i-1,j+1} - 2w_{i+1,j} + 4w_{i,j} - 2w_{i-1,j} + w_{i+1,j-1} - 2w_{i,j-1} + w_{i-1,j-1}}{h^2 k^2}, \tag{27}$$

Substituting the Eqs. (23)–(27) in the Eq. (11), and using $h = k$, we get

$$\begin{aligned} w_{i,j} = {} & A\left[w_{i+1,j} + w_{i-1,j} + w_{i,j+1} + w_{i,j-1}\right] \\ & - B\left[w_{i+2,j} + w_{i-2,j} + w_{i,j+2} + w_{i,j-2}\right] \\ & - C\left[w_{i+1,j+1} + w_{i-1,j+1} + w_{i+1,j-1} + w_{i-1,j-1}\right] + D, \end{aligned} \tag{28}$$

in which

$$A = \left[\frac{8c^2 + h^2}{h^4\sigma^2 + 4h^2 + 20c^2}\right], \quad B = \left[\frac{c^2}{h^4\sigma^2 + 4h^2 + 20c^2}\right],$$
$$C = \left[\frac{2c^2}{h^4\sigma^2 + 4h^2 + 20c^2}\right], \quad D = \left[\frac{Gh^4}{h^4\sigma^2 + 4h^2 + 20c^2}\right].$$

The boundary conditions (12)–(14) give,

$$w_{i,0} = 0 = w_{i,n} \quad \text{and} \quad 0 \leqslant i \leqslant n, \tag{29}$$

$$w_{0,j} = 0 = w_{n,j} \quad \text{and} \quad 0 \leqslant j \leqslant n, \tag{30}$$

$$w_{1,j} = w_{-1,j}, \quad w_{n+1,j} = w_{n-1,j}, \quad w_{i,-1} = w_{i,1}, \quad w_{i,n+1} = w_{i,n-1}. \tag{31}$$

The difference equation (28) gives rise to an algebraic system of equations in terms of $w_{i,j}$. The resultant algebraic system has been solved by making use of Gauss-elimination method.

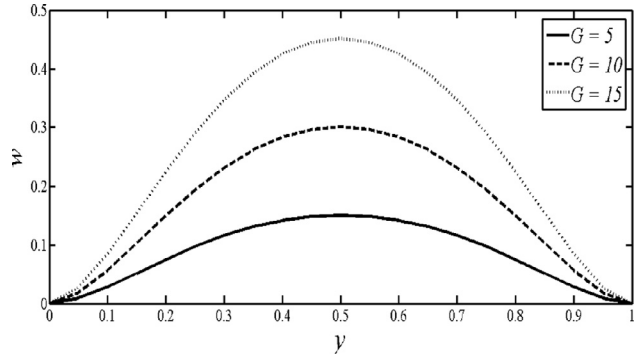

Fig. 2 Variations of velocity for various values of G when $c = 0.15$ and $\sigma = 1$ at $x = 0.5$.

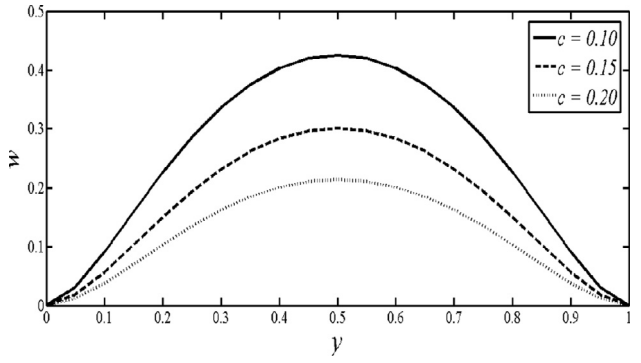

Fig. 4 Variations of velocity for various values of c when $G = 10$ and $\sigma = 1$ at $x = 0.5$.

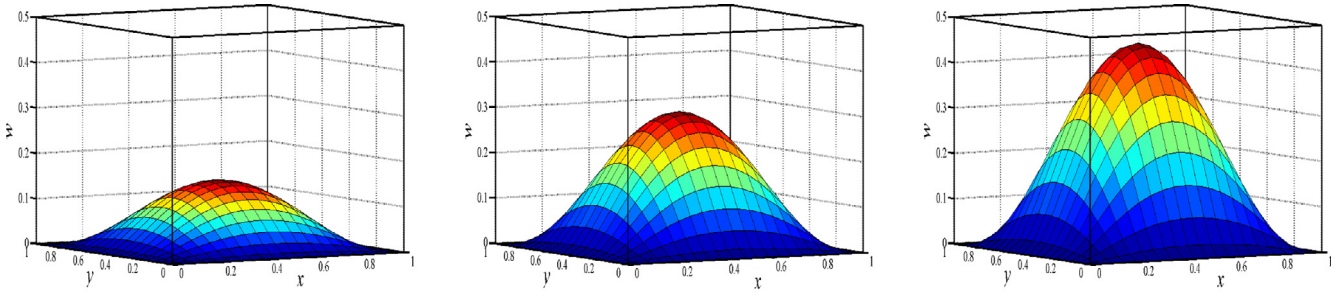

Fig. 3 Velocity profiles in 3-D for various values of G when $c = 0.15$ and $\sigma = 1$ (a) $G = 5$, (b) $G = 10$ and (c) $G = 15$.

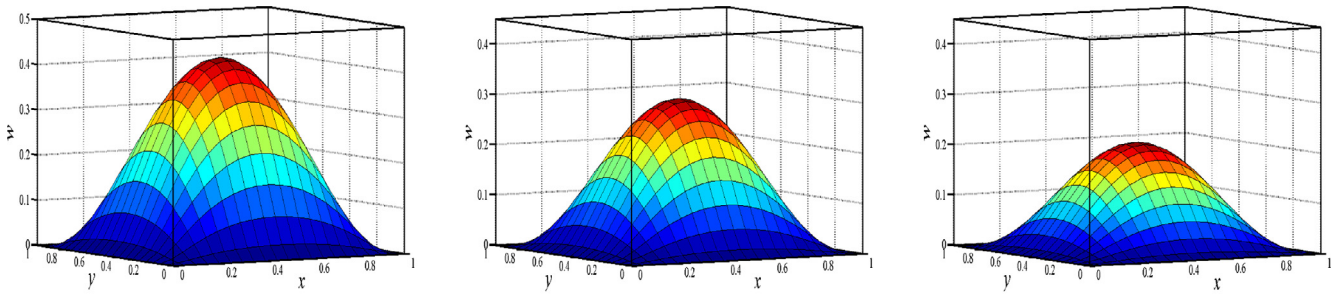

Fig. 5 Velocity profile in 3-D for various values of c when $G = 10$ and $\sigma = 1$ (a) $c = 0.1$, (b) $c = 0.15$ and (c) $c = 0.2$.

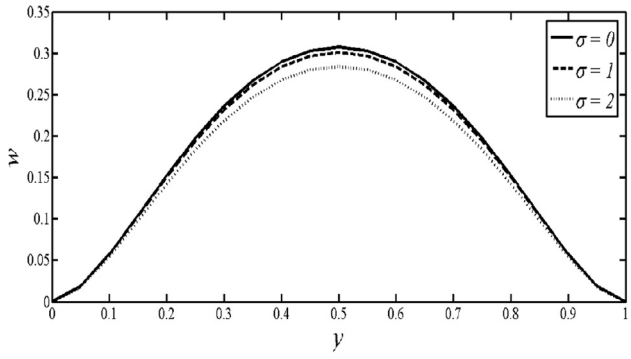

Fig. 6 Variations of velocity for various values of σ when $G = 10$ and $c = 0.15$ at $x = 0.5$.

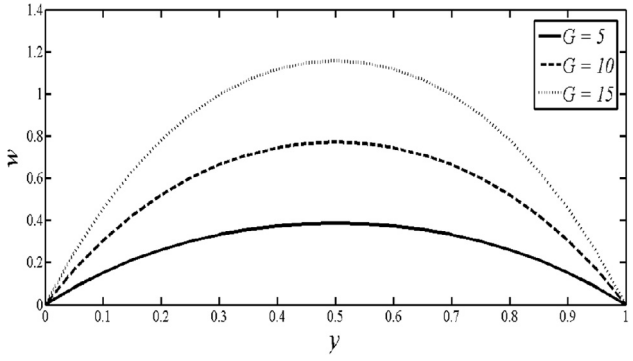

Fig. 8 Variations of velocity for various values of G when $\sigma = 0.5$ and $\lambda_1 = 0.1$ at $x = 0.5$.

3.2. *Jeffrey fluid model*

Eq. (20) along with the boundary conditions (21) and (22) are solved numerically using finite difference method. The derivatives are replaced by the central difference approximations to obtain algebraic system of equations and the classical Gauss elimination method is used to solve the resulting algebraic system of equations. Using the second order central difference approximations of the second order derivatives (23) and (24) in Eq. (20) and after simplification, we get

$$Ew_{i,j} - w_{i+1,j} - w_{i-1,j} - w_{i,j+1} - w_{i,j-1} = F, \tag{32}$$

in which

$$E = \left(4 + \sigma^2(1+\lambda_1)h^2\right) \quad \text{and} \quad F = G(1+\lambda_1)h^2.$$

The boundary conditions (21) and (22) become

$$w_{i,0} = 0 = w_{i,n} \quad \text{and} \quad 0 \leqslant i \leqslant n, \tag{33}$$

$$w_{0,j} = 0 = w_{n,j} \quad \text{and} \quad 0 \leqslant j \leqslant n, \tag{34}$$

The difference equation (32) gives us an algebraic system of equations in terms of $w_{i,j}$. This system is solved using the classical Gauss elimination method with the help of Matlab program.

4. Volume flow rate

The volume flow rate across the cross section of the duct is given as

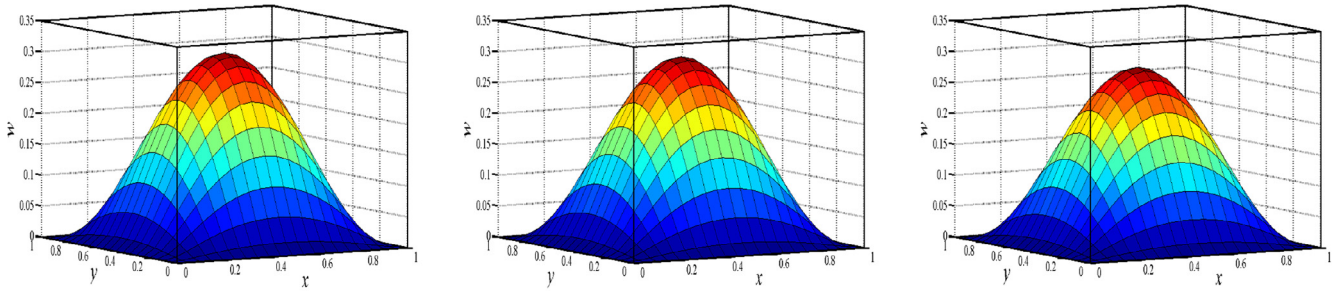

Fig. 7 Variations of velocity profile in 3-D for various values of σ when $G = 10$ and $c = 0.15$ (a) $\sigma = 0$, (b) $\sigma = 1$ and (c) $\sigma = 2$.

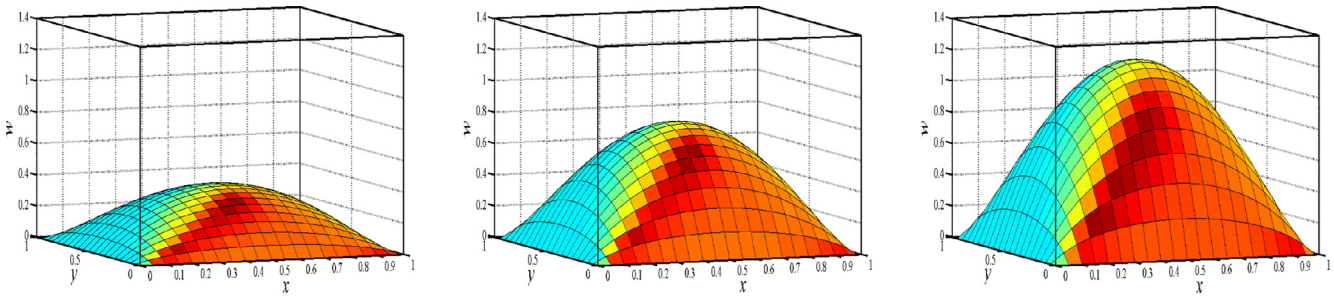

Fig. 9 Velocity profiles in 3-D for various values of G when $\lambda_1 = 0.1$ and $\sigma = 0.5$ (a) $G = 5$, (b) $G = 10$ and (c) $G = 15$.

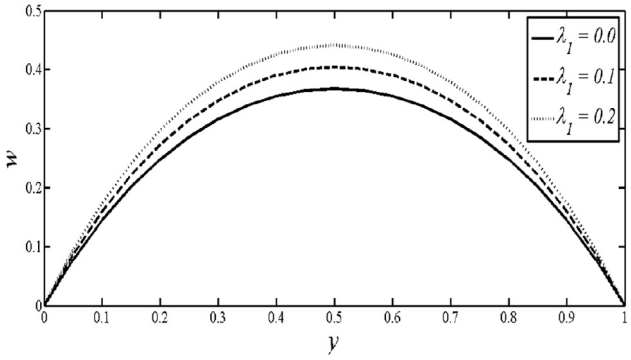

Fig. 10 Variations of velocity for various values of λ_1 when $G = 10$ and $\sigma = 0.5$ at $x = 0.5$.

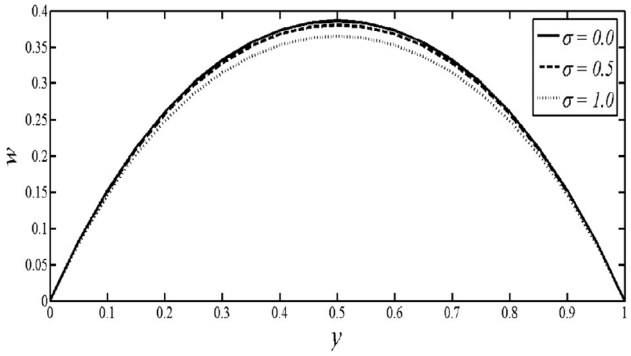

Fig. 12 Variations of velocity for various values of σ when $G = 10$ and $\lambda_1 = 0.1$ at $x = 0.5$.

$$Q = \int_0^1 \int_0^1 w(x, y)dxdy. \tag{35}$$

As the analytical solution of the velocity is not known in both the cases, the above integral is evaluated numerically to find the volume flow rate for different set of flow parameters. The effect of various parameters on the volume flow rate is presented numerically in Tables 1–3 in the case of couple stress fluid model and Tables 4–6 in the case of Jeffrey fluid model.

5. Results and discussion

In this section, we have discussed the influence of the different flow parameters on the velocity and volume flow rate. The results are graphically (two and three-dimensional) presented for the velocity profiles in Figs. 2–7 in the case of couple stress fluid and the Figs. 8–13 in the case of Jeffrey fluid. The effect of various flow parameters on the volume flow rate for couple stress fluid model and Jeffrey fluid model are respectively seen in Tables 1–3 and 4–6. It can be seen from Tables 1–3 that, the volume flow rate increases with the increasing pressure gradient while it decreases with the increasing couple stresses and porosity parameter. It is observed from Tables 4–6 that, the volume flow rate increases with the increasing pressure gradient and Jeffrey parameter while it decreases with the increasing porosity parameter. Table 7 represents the comparison of present results with the Newtonian fluid model. It is observed from this table that, the results of couple stress fluid and

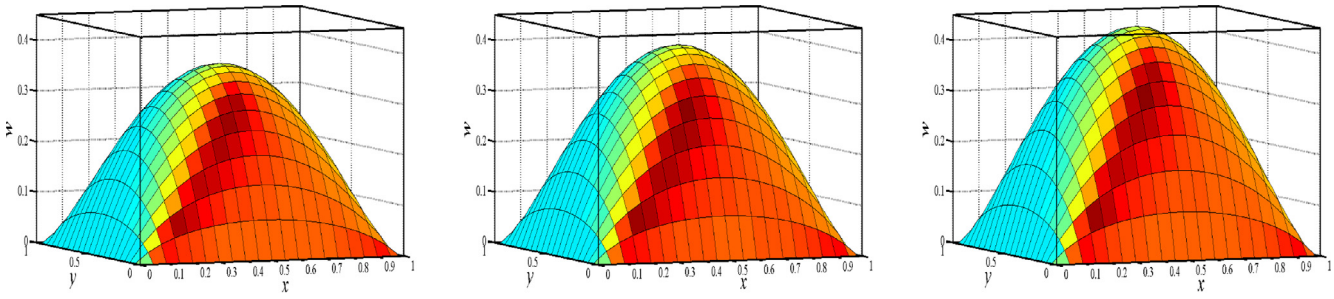

Fig. 11 Velocity profile in 3-D for various values of λ_1 when $G = 10$ and $\sigma = 0.5$ (a) $\lambda_1 = 0$, (b) $\lambda_1 = 0.1$ and (c) $\lambda_1 = 0.2$.

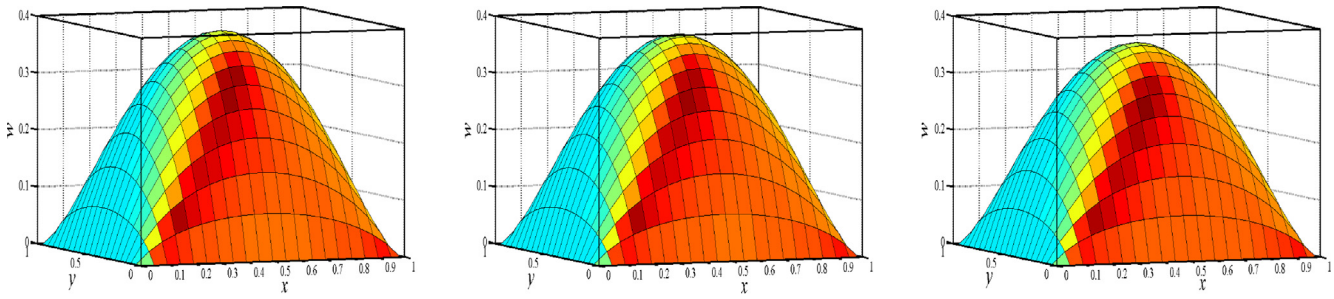

(a) (b) (c)

Fig. 13 Variations of velocity profile in 3-D for various values of σ when $G = 10$ and $\lambda_1 = 0.1$ (a) $\sigma = 0$, (b) $\sigma = 0.5$ and (c) $\sigma = 1$.

Table 1 Numerical values of the volume flow rate with the pressure gradient for $\sigma = 1$ and $c = 0.15$.

G	Q
5	0.0510
10	0.1020
15	0.1530

Table 2 Numerical values of the volume flow rate with the couple stress parameter for $G = 10$ and $\sigma = 1$.

c	Q
0.1	0.1534
0.15	0.1020
0.2	0.0703

Table 3 Numerical values of the volume flow rate with the porosity parameter for $G = 10$ and $c = 0.15$.

σ	Q
0	0.1039
1	0.1020
2	0.0967

Table 4 Numerical values of the volume flow rate with the pressure gradient for $\sigma = 0.5$ and $\lambda_1 = 0.1$.

G	Q
5	0.1892
10	0.3784
15	0.5676

Table 5 Numerical values of the volume flow rate with the Jeffrey parameter for $G = 10$ and $\sigma = 0.5$.

λ_1	Q
0	0.3444
0.1	0.3784
0.2	0.4123

Table 6 Numerical values of the volume flow rate with the porosity parameter for $G = 10$ and $\lambda_1 = 0.1$.

σ	Q
0	0.3835
0.5	0.3784
1	0.3640

Jeffrey fluid in the limiting cases are in good agreement with that of Newtonian fluid.

Figs. 2 and 3 represent the velocity profiles for different values of pressure gradient. It is clear from the figures that, the velocity increases with an increase in pressure gradient. Moreover, it is noticed that, the flow is due to the constant pressure gradient. If the pressure gradient is zero, no flow occurs. Figs. 4 and 5 give the velocity profiles for different values of couple stress parameter. It is observed from the figures that, the velocity decreases with an increase in couple stress parameter. Since $c^2 = \frac{\eta}{\mu a^2}$, c increases as the couple stress parameter η increases. Thus, an increase in couple stresses has a decreasing effect on the fluid velocity. Figs. 6 and 7 exhibit the velocity profiles for different values of porosity parameter. It is depicted from the figures that, the velocity decreases with an increase in porosity parameter. Moreover, it is noticed that, $\sigma = 0$ gives the clear medium. From this we can say that the velocity decreases from clear medium to porous medium.

Figs. 8 and 9 represent the velocity profiles for different values of pressure gradient. It is observed from these figures that, the velocity increases with an increase in pressure gradient. Moreover, as the flow is due to the constant pressure gradient only, no flow takes place if the pressure gradient is zero. Figs. 10 and 11 illustrate the variation of velocity with various values of the Jeffrey parameter λ_1. From these figures, it is depicted that, an increase in non-Newtonian parameter λ_1 increases the velocity of the fluid. It is clearly noticed from our analysis that, $\lambda_1 = 0$ gives Newtonian fluid model. Therefore, the fluid velocity increases from Newtonian to non-Newtonian fluid. Figs. 12 and 13 display the variation of velocity with various values of the porosity parameter σ. From the figures, it is seen that the velocity is a decreasing function of the porosity parameter σ. As $\sigma = 0$ gives the flow through clear medium, it can be seen that, the velocity decreases that from non-porous medium to porous medium.

Table 7 Comparison of velocity for the couple stress fluid, Jeffrey fluid and Newtonian fluid when the other parameters are fixed when $x = 0.5,\ G = 10$.

y	w (Couple stress fluid velocity when $c = 0$ and $\sigma = 0$)	w (Jeffrey fluid velocity when $\lambda_1 = 0$ and $\sigma = 0$)	Newtonian fluid velocity
0.0	0.000000000	0.000000000	0.000000000
0.1	0.290286758	0.290286758	0.290723782
0.2	0.496740178	0.496740178	0.49755873
0.3	0.633484384	0.633484384	0.634591483
0.4	0.711180317	0.711180317	0.71246492
0.5	0.736351021	0.736351021	0.737695336
0.6	0.711180317	0.711180317	0.71246492
0.7	0.633484384	0.633484384	0.634591483
0.8	0.496740178	0.496740178	0.49755873
0.9	0.290286758	0.290286758	0.290723782
1.0	0.000000000	0.000000000	0.000000000

6. Conclusions

The pressure driven steady flow of incompressible couple stress and Jeffrey fluids through porous medium in a uniform straight square duct have been studied separately. In both the problems, the numerical solution of velocity is obtained using finite difference scheme. The numerical results for the volume flow rate have been presented through tables. The results indicate that, the limiting solutions of couple stress fluid and Jeffrey fluid flows are in good agreement with that of Newtonian fluid flow. The flow characteristics are analyzed through two and three dimension plots for both the cases. It is noticed that, the velocity and volume flow rate are the increasing functions of pressure gradient. The velocity and volume flow rate are decreasing from clear medium to porous medium in both the cases. It is also observed that, an increase in the couple stress parameter decreases the fluid velocity and volume flow rate, and an increase in Jeffrey parameter increases the velocity and volume flow rate.

Conflict of interest

The authors declare that there is no conflict of interest.

Acknowledgement

The authors express their thankfulness to the anonymous reviewers and the Editor-in-Chief for the valuable suggestions which led to the improvement of the quality of the paper.

Appendix A.

The governing equation for the flow of Newtonian fluid through duct of uniformly square cross section is given by

$$\mu\nabla^2 w - \frac{\partial p}{\partial z} = 0, \tag{36}$$

with the boundary conditions

$$w(x,0) = 0 = w(x,a) \quad \text{for } 0 \leqslant x \leqslant a, \tag{37}$$

$$w(0,y) = 0 = w(a,y) \quad \text{for } 0 \leqslant y \leqslant a. \tag{38}$$

Using the non-dimensional scheme (10), the Eqs. (36)–(38) become,

$$\nabla^2 w + G = 0, \tag{39}$$

with the boundary conditions

$$w(x,0) = 0 = w(x,1) \quad \text{for } 0 \leqslant x \leqslant 1, \tag{40}$$

$$w(0,y) = 0 = w(1,y) \quad \text{for } 0 \leqslant y \leqslant 1. \tag{41}$$

Using the method of separation of variables, the solution of Eq. (39) with boundary conditions (40) and (41) is obtained as

$$w(x,y) = \frac{G}{2}\left[y(1-y) - \sum_{k=1}^{\infty} \frac{8}{(2k-1)^3\pi^3}\left\{\cosh[(2k-1)\pi x] + (1-\cosh[(2k-1)\pi])\frac{\sinh[(2k-1)\pi x]}{\sinh[(2k-1)\pi]}\right\}\sin[(2k-1)\pi y]\right]. \tag{42}$$

This velocity field for the Newtonian fluid case has been used to compare the results of limiting solutions of couple stress and Jeffrey fluids.

References

Adachi, T., 2006. Stability of natural convection in an inclined square duct with perfectly conducting side walls. Int. J. Heat Mass Transfer 49, 2372–2380.

Afifi, N.A.S., Gad, N.S., 2001. Interaction of peristaltic flow with pulsatile magneto-fluid through a porous medium. Acta Mech. 149, 229–237.

Akbar, N.S., Nadeem, S., 2012. Simulation of variable viscosity and Jeffrey fluid model for blood flow through a tapered artery with a stenosis. Commun. Theor. Phys. 57, 133–140.

Beale, S.B., 2005. Mass transfer in plane and square ducts. Int. J. Heat Mass Transfer 48, 3256–3260.

Cook, A.E., Rahman, M., 1986. Temperature and velocity distributions in a square duct. Appl. Math. Model. 10, 221–223.

Devakar, M., 2013. MHD effects on the unsteady flow of a couple stress fluid due to the sudden motion of an infinite flat plate. Eur. J. Sci. Res. 94 (4), 398–405.

Devakar, M., Iyengar, T.K.V., 2008. Stokes' problems for an incompressible couple stress fluid. Nonlinear Anal. Model. Control 13 (2), 181–190.

Devakar, M., Iyengar, T.K.V., 2010. Run up flow of an incompressible couple stress fluid between parallel plates. Non-Linear Anal. Model. Control 15 (1), 29–37.

Devakar, M., Sreenivasu, D., Shankar, B., 2014. Analytical solutions of couple stress fluid flows with slip boundary conditions. Alexandria Eng. J. 53 (3), 723–730.
Ellahi, R., 2013. The effects of MHD and temperature dependent viscosity on the flow of non-Newtonian nanofluid in a pipe: analytical solutions. Appl. Math. Model. 37 (3), 1451–1467.
Ellahi, R., 2014. The thermodynamics, stability, applications and techniques of differential type: a review. Rev. Theor. Sci. 2 (2), 116–123.
Ellahi, R., Aziz, S., Zeeshan, A., 2013. Non-Newtonian nanofluid flow through a porous medium between two coaxial cylinders with heat transfer and variable viscosity. J. Porous Media 16 (3), 205–216.
Farooq, M., Rahim, M.T., Islam, S., Siddiqui, A.M., 2013. Steady Poiseuille flow and heat transfer of couple stress fluids between two parallel inclined plates with variable viscosity. J. Assoc. Arab Univ. Basic Appl. Sci. 14, 9–18.
Fetecau, C., Fetecau, Corina, 2005. Unsteady flows of Oldroyd-B fluids in a channel of rectangular cross-section. Int. J. Non-Linear Mech. 40, 1214–1219.
Firouzi, M., Hashemabadi, S.H., 2009. Exact solution of two phase stratified flow through the pipes for non-Newtonian Herschel–Bulkley fluids. Int. Commun. Heat Mass Transfer 36, 768–775.
Hayat, T., Awais, M., Asghar, S., 2013a. Radiative effects in a three-dimensional flow of MHD Eyring–Powell fluid. J. Egypt. Math. Soc. 21, 379–384.
Hayat, T., Shehzad, S.A., Alsaedi, A., 2013b. Three-dimensional stretched flow of Jeffrey fluid with variable thermal conductivity and thermal radiation. Appl. Math. Mech. Engl. Ed. 34 (7), 823–832.
Heris, S.Z., Nassan, T.H., Noie, S.H., 2011. CuO/water nanofluid convective heat transfer through square duct under uniform heat flux. Int. J. Nanosci. Nanotechnol. 7 (3), 111–120.
Johnson, R.W., 1998. The Handbook of Fluid Dynamics. Springer Science & Business Media.
Khan, M., Anjum, Asia, Fetecau, C., Qi, Haitao, 2010. Exact solutions for some oscillating motions of a fractional Burgers' fluid. Math. Comput. Model. 51, 682–692.
Kothandapani, M., Srinivas, S., 2008. Peristaltic transport of a Jeffrey fluid under the effect of magnetic field in an asymmetric channel. Int. J. Non-Linear Mech. 43, 915–924.
Kun, M.A., Shiwei, Yuan, Huaijian, Chang, Huanxin, Lai, 2014. Experimental study of pseudoplastic fluid flows in a square duct of strong curvature. J. Therm. Sci. 23 (4), 359–367.
Lee, S.H., 2008. Convective heat transfer to water near the critical region in a horizontal square duct. Int. J. Heat Mass Transfer 51, 2930–2939.
Liu, Q.S., Jian, Y.J., Yang, L.G., 2011. Time periodic electroosmotic flow of the generalized Maxwell fluids between two micro-parallel plates. J. Non-Newtonian Fluid Mech. 166, 478–486.
Mukhopadhyay, Swati, Bhattacharyya, Krishnendu, 2012. Unsteady flow of a Maxwell fluid over a stretching surface in presence of chemical reaction. J. Egypt. Math. Soc. 20, 229–234.
Murthy, P.V.S.N., Srinivasacharya, D., Krishna, P.V.S.S.S.R., 2004. Effect of double stratification on free convection in darcian porous medium. Trans. ASME J. Heat Transfer 126 (2), 297–300.
Nadeem, S., Akram, Safia, 2010. Peristaltic flow of a Jeffrey fluid in a rectangular duct. Nonlinear Anal. Real World Appl. 11, 4238–4247.
Norouzi, M., Kayhani, M.H., Shu, C., Nobari, M.R.H., 2010. Flow of second-order fluid in a curved duct with square cross-section. J. Non-Newtonian Fluid Mech. 165, 323–339.
Prasad, B.G., Kumar, Amit, 2011. Flow of a hydromagnetic fluid through porous media between permeable beds under exponentially decaying pressure gradient. Comput. Methods Sci. Technol. 17 (2), 63–74.
Qayyum, A., Awais, M., Alsaedi, A., Hayat, T., 2012. Unsteady squeezing flow of Jeffery fluid between two parallel disks. Chin. Phys. Lett. 29 (3), 034701.
Radhakrishnamacharya, G., 1977. Flow of micropolar fluid through a constricted channel. Int. J. Eng. Sci. 15, 719–725.
Rahman, M., Ahmad, S.Y., 1982. Finite element analysis of axial flow with heat transfer in a square duct. Appl. Math. Model. 6, 481–490.
Ramana Murthy, J.V., Muthu, P., Nagaraju, G., 2010. Finite difference solution for MHD flow of couple stress fluid between two concentric rotating cylinders with porous lining. IJAMM 6 (12), 1–28.
Ramesh, K., Devakar, M., 2015. Magnetohydrodynamic peristaltic transport of couple stress fluid through porous medium in an inclined asymmetric channel with heat transfer. J. Magn. Magn. Mater. 394, 335–348.
Rao, I.J., 1999. Flow of a Johnson–Segalman fluid between rotating co-axial cylinders with and without suction. Int. J. Non-Linear Mech. 34, 63–70.
Sarma, D., Deka, P.N., Kakaty, S.C., 2014. Numerical study of liquid metal mhd flow through a square duct. Asian J. Current Eng. Maths 3 (2), 15–19.
Sayed-Ahmed, M.E., 2000. Laminar heat transfer for thermally developing flow of a Herschel-Bulkley fluid in a square duct. Int. Commun. Heat Mass Transfer 27 (7), 1013–1024.
Sheikholeslami, M., Ellahi, R., Ashorynejad, H.R., Domairry, G., Hayat, T., 2014. Effects of heat transfer in flow of nanofluids over a permeable stretching wall in a porous medium. J. Comput. Theor. Nanosci. 11 (2), 486–496.
Srinivasacharya, D., Srinivasacharyulu, N., Ojjela, Odelu, 2009. Flow and heat transfer of couple stress fluid in a porous channel with expanding and contracting wall. Int. Commun. Heat Mass Transfer 36, 180–185.
Stokes, V.K., 1984. Theories of Fluids with Microstructure. Springer, New York.
Ting, H.H., Hou, S.S., 2015. Investigation of laminar convective heat transfer for Al_2O_3-water nanofluids flowing through a square cross-section duct with a constant heat flux. Materials 8, 5321–5335.
Tripathi, D., 2002. Peristaltic hemodynamic flow of couple stress fluid through a porous medium with slip effect. Transp. Porous Med. 92, 559–572.
Tympel, S., Krasnov, D., Boeck, T., Schumacher, J., 2012. Distortion of liquid metal flow in a square duct due to the influence of a magnetic point dipole. Proc. Appl. Math. Mech. 12, 567–568.
Vajravelu, K., Cannon, J.R., Rollins, D., Leto, J., 2002. On solutions of some non-linear differential equations arising in third grade fluid flows. Int. J. Eng. Sci. 40, 1791–1805.
Zeeshan, A., Ellahi, R., 2013. Series solutions for nonlinear partial differential equations with slip boundary conditions for non-Newtonian MHD fluid in porous space. Appl. Math. Inf. Sci. 7 (1), 257–265.
Zhang, M., Shen, X., Ma, J., Zhang, B., 2007. Numerical study of flow of Oldroyd-3-Constant fluids in a straight duct with square cross-section. Korea-Australia Rheol. J. 19 (2), 67–73.